Earthquake Geotechnical Engineering for Protection and Development of Environment and Constructions – Silvestri & Moraci (Eds)
© 2019 Associazione Geotecnica Italiana, Rome, Italy, ISBN 978-0-367-14328-2

Estimation of ground amplification factors in a mountain district using earthquake observations and three-dimensional FEM analyses

H. Sakai
Hosei University, Tokyo, Japan

Y. Fujinami
Tokyo Metropolitan Government, Tokyo, Japan

M. Yoshimi
National Institute of Advanced Industrial Science and Technology, Ibaraki, Japan

K. Sato
Central Research Institute of Electric Power Industry, Chiba, Japan

ABSTRACT: We observed microtremors and earthquakes and performed Swedish weight sounding tests at a hill to investigate the seismic amplification by mountain topography. We also conducted earthquake response analyses of the hill based on three-dimensional finite element methods (FEMs). The amplification characteristics from the three-dimensional finite element (FE) analyses agreed well with those from the observations over most of the frequency range. The fundamental natural period of the hill was nearly identical to the one calculated as a uniform fixed-free shear beam, assuming a beam length equal to the height of the hill. This result suggests that the fundamental natural period of elevated topographic features can be calculated with comparative ease, which is consistent with the results of Cauzzi et al. (2012). Finally, the seismic amplification around the fundamental natural period was observed to increase with increased altitude of the observation site.

1 INTRODUCTION

Topography is one of the key factors that cause amplification of the earthquake ground motion. Since approximately 70% of Japanese lands are classified as montane, topographic effect on the ground motion is of great issue for seismic hazard assessment as landslides and/or slope failure have aggravated earthquake disasters. Topographic effect is somehow considered in seismic hazard assessment because an amplification factor for seismic intensity indexes such as Fujimoto & Midorikawa (2003) considers elevation and the slope gradient in regression analysis. However, as the topographic effect is a result of complicated response of an irregular ground like mountains and hills, observation and numerical analysis are important.

Bouchon & Barker (1996) performed numerical simulations of a small hill during aftershocks of the 1994 Northridge earthquake in California. The results of these simulations indicated that the topography of the site amplified the large east–west accelerations recorded there during the Northridge mainshock by 30–40%. However, they could not fully explain the amplitude of the effects observed.

Part 5 of Eurocode 8 (European Committee for Standardization, 1994) provided the amplification factors that ranged from 1.2–1.4 and differed by the slope angle of the topographic feature. The code indicates that the amplification factor may be assumed to decrease as a linear function of the height above the base of a cliff or ridge, and to be in unity at the base.

Paolucci (2002) theoretically derived the fundamental vibration frequency of a homogeneous triangular mountain. He also estimated the amplification factor for several steep, topographically irregular sites based on two- and three-dimensional numerical analyses, and showed that some of the amplification factors from three-dimensional analyses were larger than the ones recommended by Eurocode 8.

Ma et al. (2007) investigated the effects of large-scale surface topography on ground motions generated by the nearby San Andreas Fault, based on numerical simulations. They revealed that the mountains reduced the peak amplitude of ground velocity for some regions in the basin by as much as 50% in the frequency band up to 0.5 Hz. Kurita et al. (2005) conducted three-dimensional earthquake response analyses for a small hill, as well as earthquake observations. From their results, they showed that the amplification factors around the top of the mountain were extremely large and the amplification characteristics depended upon the topography. Cauzzi et al. (2012) investigated the topographic amplification and the predominant period based on numerical simulations and earthquake observations. They found that mountain topography was segregated into several configuration types and the dominant period could be estimated for these types. However, previous studies, including the aforementioned, have not yet fully clarified the amplification characteristics of mountain topography. Therefore, we perform microtremor and earthquake observations at a small hill and numerical simulations for three observed earthquakes

2 FIELD TESTS

2.1 *Earthquake and microtremor observations*

We conducted earthquake and microtremor observations at a small hill in Yokosuka City, Kanagawa, Japan, located 52 km south of Tokyo, on December 1 and 2 of 2015. The height of the hill is 55 m and it is comprised of a nearly homogeneous sandstone. The hill has one cave, which we can observe microtremors and earthquakes in, is suitable for studying the aseismic amplification of mountain topography. The eight measurements sites from this study are shown in Figure 1. We used 7 records of the observation sites from ZDY00 to ZDY06, which were located at the hill. Another unused site, ZDY10, is on an adjacent, flat, reclaimed ground layer. Sites ZDY01–ZDY06 are on the surface of the hill; ZDY00 is in the cave and ZDY06 is on the top of the hill, located along the same position of flat plane as ZDY00. We deployed the measurement instruments on the sandstone outcrop from ZDY00–ZDY04, and on the surface of the sediment layer at ZDY05 and ZDY06. The differences in elevation among the observation sites relative to ZDY00 are shown in Table 1. In Figure 2, we show the horizontal-to-vertical spectral ratio at the ZDY05 and ZDY06 sites. As is apparent from Figure 2, the dominant frequencies at ZDY05 and ZDY06 are approximately 8–9 Hz and 8–10 Hz, respectively.

We were able to measure three earthquakes on December 2 in 2015. The profiles of the earthquakes are shown in Table 2. The maximum velocity ratios of each site to ZDY00 are shown in Table 3, and the relationships between the height from ZDY00 and the geometric mean of the amplification ratio at each site relative to ZDY00 are depicted in Figure 3. From Table 3 and

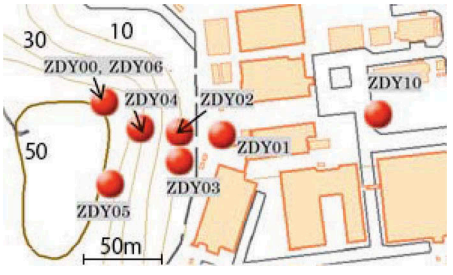

Figure 1. Location of the earthquake and microtremor observation sites. (bold and thin curve lines denote a topographic contour line)

Table 1. Elevation differences bween the observation sites and site ZDY00

Site No.	Elevation difference (m)
ZDY01	0.7
ZDY02	13.6
ZDY03	19.3
ZDY04	34.4
ZDY05	45.2
ZDY06	46.8

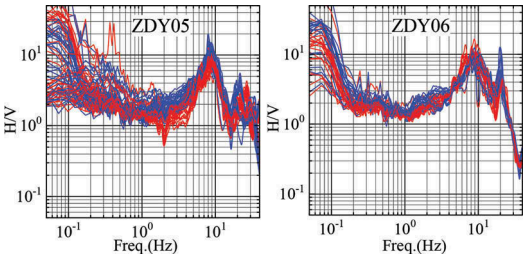

Figure 2. Horizontal-to-vertical spectral ratio (H/V)

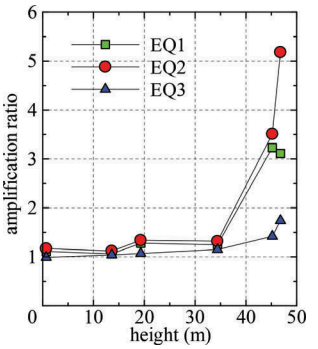

Figure 3. Relationships between the height from ZDY00 and the geometric mean of the amplification ratio at each site against ZDY00

Table 2. Profiles of three earthquakes

No.	Time of occurrence	Magnitude (JMA)	Epicenter
1	01:07:15 am.	3.8	South of Ibaraki
2	03:26:40 am.	2.7	Center of Chiba
3	07:49:06 am.	4.6	Off-Miyagi

Table 3. Maximum velocity ratio of each observation site to ZDY00

Earthquake No.	Component	ZDY01	ZDY02	ZDY03	ZDY04	ZDY05	ZDY06
1	NS	1.12	0.96	1.16	1.05	2.51	2.51
	EW	1.11	1.18	1.41	1.50	4.16	3.85
	UD	1.00	1.11	1.20	1.27	1.60	1.49
2	NS	1.04	1.13	1.26	1.05	2.49	4.61
	EW	1.32	1.11	1.42	1.67	4.97	5.82
	UD	1.55	1.13	1.11	1.35	1.31	1.30
3	NS	0.97	1.14	1.13	1.18	1.33	1.79
	EW	1.02	0.95	1.02	1.12	1.53	1.71
	UD	1.04	0.96	1.05	1.06	0.96	1.08

Figure 3, we can observe that the maximum velocity ratios of E–W and N–S components tend to be larger as the elevation increases. Eurocode 8 notes that the value of the simplified topographic amplification factor may be assumed to decrease as a linear function of the height above the base of a cliff or ridge. The relationships between the height and amplification ratio at the sites ZDY01–ZDY04 correspond well with the trend noted in Eurocode 8, especially with respect to the data for earthquake 3, which exhibits an approximately linear relationship. However, the ratios of the E–W and N–S components of ZDY05 and ZDY06 are much larger than the others for all three earthquakes, and the trend is not coincident with the one written in Eurocode 8. As an example, we show the velocity records of the E–W components of earthquake 1 in Figure 4. As is apparent from this figure, the amplitudes of the velocity at the sites ZDY05 and ZDY06 are larger than those at the other sites. This tendency to amplify is the same for the other earthquakes and for the N–S components. We consider that the major reason for these trends is the existence of a soft surface sediment layer at sites ZDY05 and ZDY06. Therefore, we conducted sounding tests at both sites to determine the ground conditions.

2.2 *Sounding test*

Observation sites ZDY05 and ZDY06 are located at the top of the hill, where the soft soils cover the sandstone composing the hill. We conducted Swedish weight sounding tests twice at

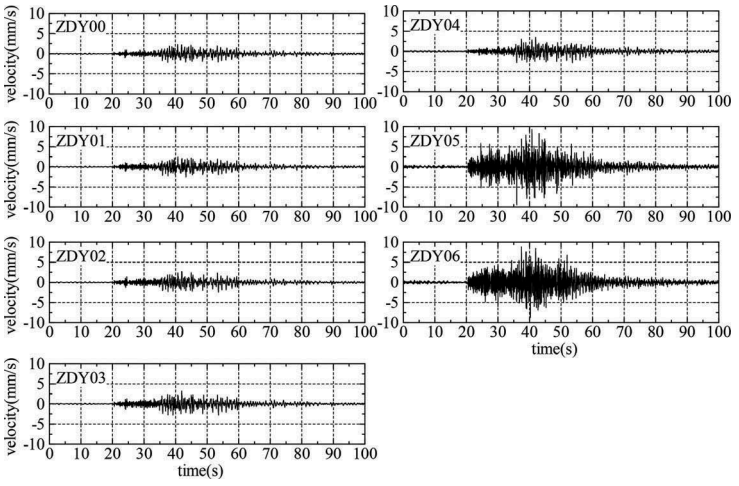

Figure 4. Observed velocity record waveforms (E–W components of earthquake 1)

Table 4. Properties of surface layers

Site No.	Test No.	Thickness (m)	Conversion N-value
ZDY05	1	4.1	2.5
	2	4.2	2.5
ZDY06	1	4.4	2.8
	2	4.3	2.8

each site to investigate the thickness and the shear velocity of the surface layer on December 11, 2017. The surface soil was estimated to be an organic clay based on the noise during the sounding tests. The thickness and conversion N-value are shown in Table 4.

The mean shear velocity of the surface sediment layer is estimated to 138 m/s from the N-values in Table 4, using the empirical relationship presented in the Japanese specifications for highway bridges. The fundamental frequency of the surface layer is calculated as 8.3 Hz, based on the theory of uniform fixed-free shear beam vibrations (e.g., Blevins, 1979). The natural frequencies, f_i, are calculated using the following equation:

$$f_i = \frac{(2i-1)}{4H} Vs, \quad i = 1, 2, 3 \cdots \tag{1}$$

where H is the shear beam length (the thickness of the sediment layer) as Vs is the shear velocity. As is shown in Figure 2, the observed predominant frequencies of the sites ZDY05 and ZDY06 are 8–9 Hz and 8–10 Hz, respectively. The predominant frequency of the surface sediment layer on a rock outcrop can be calculated from equation (1) as an idealized, uniform, fixed-free shear beam.

3 NUMERICAL ANALYSES

We conducted three-dimensional FEM analysis of the hill during three earthquakes to investigate the amplification characteristics.

3.1 *Analytic model*

Two FE models of the hill are constructed. One model (model 1) has sandstone and a surface sediment layer, while the other model (model 2) the surface sediment layer is neglected. Dimension of the models are same: horizontal dimensions is 830 m in the N–S direction,

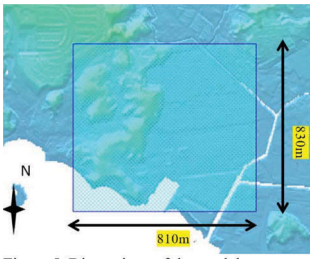

Figure 5. Dimensions of the models

Table 5. Material profiles of the model

	Shear velocity (m/s)	Density (t/m^3)	Poisson's ratio
Surface sediment layer	138	1.5	0.45
Over GL-40m	600	1.9	0.25
Under GL-40m	850	2.1	0.20

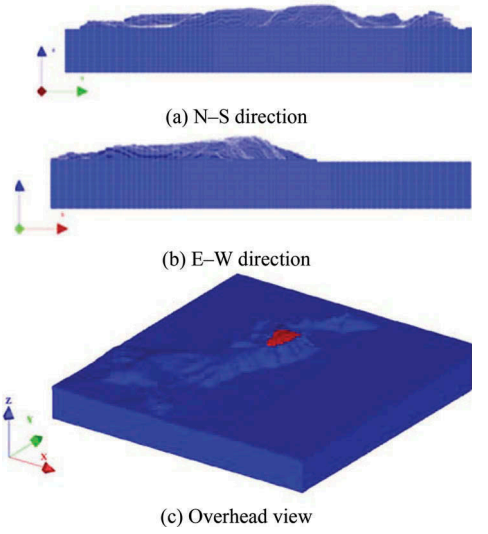

Figure 6. Analytical model. The red areas denote sediment layers

810 m in the E–W direction, and 90 m in depth direction (Figure 5). The view of the models is shown in Figure 6. The mesh sizes of the sandstone are 5 m, 10 m and 15 m, and that of the surface sediment layer is 1 m in depth for securing the analytic accuracy under a frequency of 20 Hz. Smaller mesh is adopted for the hill to assure fine topography modelling. Viscous boundary is considered on the bottom of the model, and horizontal rollers are applied on the lateral boundaries. The material properties of the hill are determined from the results of P-S logging at the site and the subsurface structure model provided by the Japan Seismic Hazard Information Station (J-SHIS), National Research Institute for Earth Science and Disaster Resilience. The material profiles of the model are shown in Table 5.

3.2 *Earthquake response analyses*

Earthquake response analyses are conducted for three small earthquakes observed on December 2, 2015. The earthquake response analysis code 7s-3 is used developed by Toki et al. (2007). Incident seismic waves at the bottom are estimated by deconvolution of the records at the ZDY00 site, using DYNEQ v.3.36. As amplitudes of the observed ground motions for the three earthquakes are small, the dynamic property of all soils is considered to be linear.

In Figures 7 and 8, the response velocity waveform and spectral ratio of the E–W component of earthquake No.2 are shown. The velocity waveform calculated at site ZDY00 should be very similar to the one from observation. However, the response velocity overestimates the observed velocity. Then for other sites, though the phases of the waveforms agree well, amplitudes of the calculated waveforms are up to about twice of the observations. This might be because the incident wave has been calculated with a one-dimensional model, whereas the response velocity is evaluated with a three-dimensional model.

The amplification ratios of model 1 and 2 are close to the observed ones at the period range shorter than 0.6 seconds (Figure 8). The ratios of model 1 agrees better to the observations than those of the model 2. Especially at the sites ZDY05 and ZDY06, the amplification ratios of the model 1 agrees much better than those of model 2 at the period range of 0.05–0.4 seconds. These results indicate that the amplification of the short-period components at sites ZDY05 and ZDY06 are mainly due to the surface sediment layer.

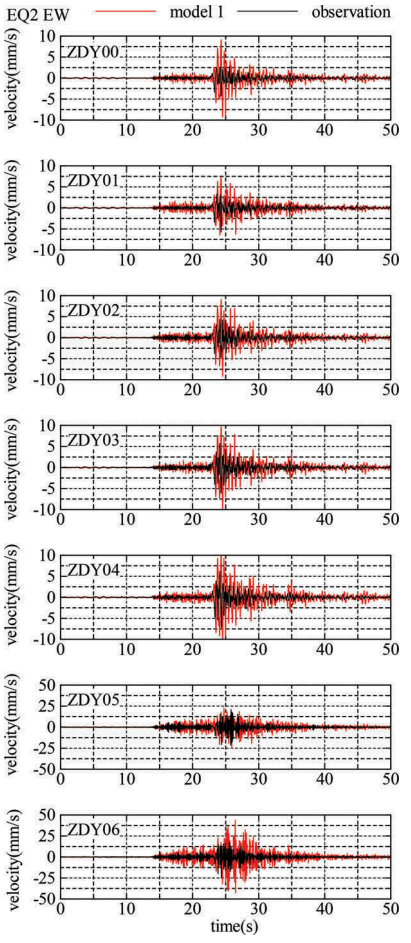

Figure 7. Calculated (model 1) and observed velocities (E–W components of earthquake 2)

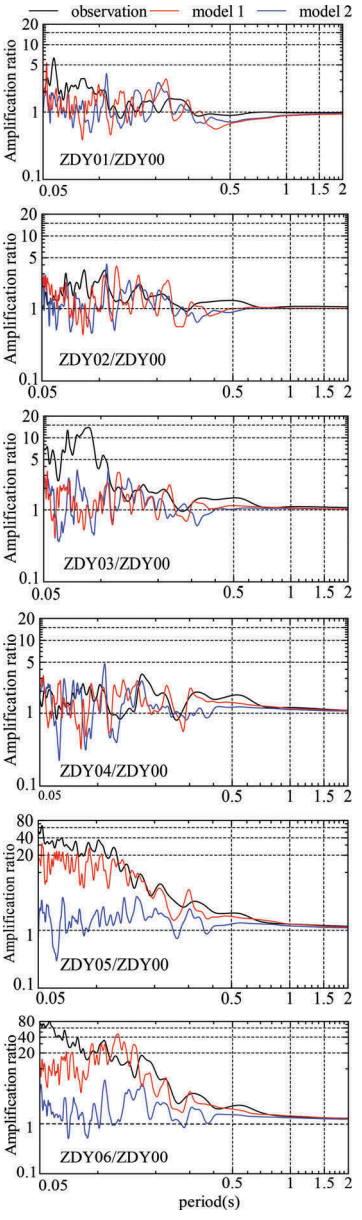

Figure 8. Calculated and observed amplification ratio of site velocities to those at site ZDY00 (E–W component of earthquake 2)

The topographic amplification ratios of components of earthquake 2 and ZDY00 at 6 observation sites are shown in Figure 9 for observed data (9a) and for analysis results (9b). Predominant periods of the hill can be recognized as 0.3 and 0.6 seconds, because the magnitude of the observed amplification (Figure 9a) increases as increase of the elevation at those periods.

Observed predominant period at 0.6 second is not reproduced by the FEM analysis, despite the fact that the amplitudes of the amplification factors at sites ZDY04–ZDY06 are close to those observed. On the other hand, at the period about 0.3 second, the FEM result reproduces

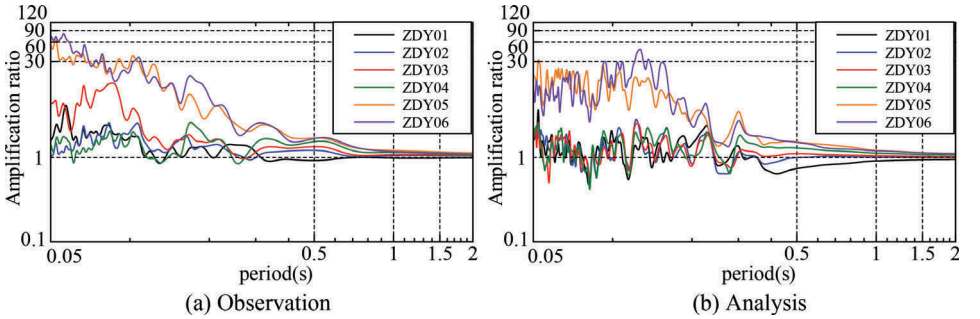

Figure 9. Topographic amplification ratios for each observation site to site ZDY00 (E–W component of earthquake 2). Assuming the height of the hill to be equal to H in equation (1), the fundamental natural period calculated is 0.37 seconds, and the predominant period from the H/V ratio is 0.1–0.125 seconds

the topographic amplification characteristics (Figure 9b) convincing that the period is one of the predominant periods of the hill. Assuming the height of the hill to be equal to H in equation (1), the fundamental natural period is calculated to be 0.37 seconds.

4 CONCLUSIONS

We used microtremor and earthquake observations, along with Swedish weight sounding tests, from a hill to investigate the seismic amplification of mountain topography. We also analysed earthquake responses based on three-dimensional FEMs and applied to observations from the hill. Our primary results are summarized below.

1. Based on earthquake observations, seismic amplification with a period of 0.2–0.5 seconds, which is considered to be the fundamental natural period of the hill, increased as the observation site ascended in altitude.
2. Amplification characteristics from the three-dimensional FE analyses agreed well with those from observations across most of the frequency range.
3. The fundamental natural period of the hill obtained from the observations and analyses was nearly the same as the one calculated from equation (1) and based on an idealized uniform fixed-free shear beam vibration, with the beam length assumed to be equal to the height of the hill, suggesting that the fundamental natural period of a mountain can be calculated directly from the equation.
4. The fundamental natural period of the surface sediment layer calculated from equation (1) coincided well with the results of the H/V spectrum based on microtremor observations.
5. Results of (1) and (3) are consistent with those of Cauzzi et al. (2012).

ACKNOWLEDGEMENTS

We are thankful to H. Kishimoto and H. Furukawa from Japan Computer Consultant, who provided three-dimensional FE analysis code and kind advice on our numerical analyses. Dr. Y. Ikeda also supported the generation of numerical models and analyses. This research was funded by the Japanese Society for the Promotion of Science (JSPS) Grants-in-Aid (KAKENHI) [Grant number 17K01343].

REFERENCES

Blevins, R.D. 1979. Formulas for natural frequency and mode shape. *Van Nostrand Reinhold*. New York.

Bouchon, M. & Barker, J.S. 1996. Seismic response of a hill: the example of Tarzana, California. *Bulletin of the Seismological Society of America* 86: 66–72.

Cauzzi, C., Faccioli, E., Stupazzini, M. & Villani, M. 2010. Including topographic amplification factors in GMPEs by means of 3D simulations of ground motions. *Proceedings of 14th European Conference of Earthquake Engineering*: Paper No. 1382. Ohrid.

Cauzzi, C., Fah, D., Pessina, V., Faccioli, E. & Smerzini C. 2012. Topographic amplification from recorded earthquake data and numerical simulations. *Proceedings of 15th World Conference on Earthquake Engineering*: Paper No. 5823. Lisbon.

CEN European Committee for Standardization 1994. *Eurocode 8. Design Provisions for Earthquake Resistance of Structures – Part 5: Foundations, Retaining Structures and Geotechnical Aspects*. ENV 1998–1995. Brussels.

Fujimoto, *K. & Midorikawa*, *S.* 2003. Average shear-wave velocity mapping throughout Japan using the Digital National Land Information, *Journal of Japan Association for Earthquake Engineering* 3(3): 13–27. [In Japanese]

Japan Road Association 2016. Specification for highway bridges – Part V: Seismic Design – ver. 2012. Tokyo.

Kurita, T., Annaka, T., Shimada, M. & Suehiro, T. 2005. Effect of irregular topography on strong ground motion amplification. *Journal of Japan Association for Earthquake Engineering* 5(3): 1–11. doi: doi.org/10.5610/jaee.5.3_1 [In Japanese]

Ma, S., Archuleta, R.J. & Page, M.T. 2007. Effects of large-scale surface topography on ground motions, as demonstrated by a study of the San Gabriel Mountains, Los Angeles, California. *Bulletin of the Seismological Society of America* 97: 2066–2079. doi: 10.1785/0120070040

Paolucci, R. 2002. Amplification of earthquake ground motion by steep topographic irregularities. *Earthquake Engineering and Structural Dynamics* 31: 1831–1853. doi: doi.org/10.1002/eqe.192

Toki, K., Kishimoto, H., Furukawa, H. & Sakai, H. 2007. Strong ground motion prediction based on 3-dimensional non-elastic FEM in Kyoto Basin area from a scenario earthquake of the Hanaore Fault. *Journal of Japan Association for Earthquake Engineering* 7(5): 45–59. [In Japanese]

Yoshida, N. 1995. DYNEQ – A computer program for dynamic response analysis of level ground equivalent linear method. https://www.kiso.co.jp/yoshida/Japanese_02.html (accessed 26 October 2015).